THE JOURNAL OF PHYSICAL CHEMISTRY C

Article

pubs.acs.org/JPCC

Explanation of Surface-Enhanced Raman Scattering Intensities of *p*-Aminobenzenethiol by Density Functional Computations

Vít Novák,[†,‡] Marcela Dendisová,[‡] Pavel Matějka,[‡] and Petr Bouř*[,†,‡]

[†]Institute of Organic Chemistry and Biochemistry, Academy of Sciences, Flemingovo náměstí 2, Prague 6, 16610, Czech Republic
[‡]University of Chemistry and Technology, Prague, Technická 5, Prague 6, 166 28, Czech Republic

Supporting Information

ABSTRACT: *p*-Aminobenzenethiol (ABT) is a popular molecule for surface-enhanced Raman scattering experiments (SERS), providing large signal enhancements on a range of metal surfaces. However, SERS intensities vary very much according to experimental conditions, and the interplay between ABT protonation, polymer state, and electronic structure/Raman cross section is still not completely clear. To understand main factors affecting Raman intensities, density functional theory (DFT) and matrix polarization theory (MPT) models were used to generate the spectra and compare to the experiment. The simulations showed that ABT protonation as well as its binding to the metal surface shift the absorption threshold, which invokes resonance or preresonance conditions favorable to the signal enhancement. The MPT approximation enabled modeling of the effect of the metal bulk and orientation of the dye on the metal surface on the enhancement and relative band intensities. The simulations can be done relatively easily and reveal chemical changes and system geometry important in rational design of SERS molecular sensors.

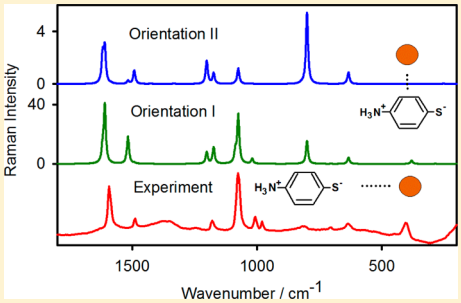

INTRODUCTION

Since its discovery,[1] surface-enhanced Raman scattering (SERS) developed for many techniques broadly used in analytical chemistry and spectral imaging.[2] For molecules placed in proximity of a noble metal, the surface Raman cross section can increase up to several orders in magnitude. In general, the interaction with the surface is difficult to control, and the enhancement strongly depends on experimental conditions. In the past, Matejka et al. proposed control of the absorption process of *p*-aminobenzenethiol (ABT) dye on Au, Ag, and Cu surfaces via the electrochemical potential of the metal plates.[3−5] On metal surfaces, ABT is supposed to form self-assembled monolayers, attached via the thiol group.[6,7]

Various computational models were previously used to interpret ABT SERS spectra,[8−10] which, however, mostly dealt with qualitative aspects of the event, such as vibrational mode assignment. Enhancement factors for the modes of the b_2 symmetry were found to be higher than those for a_1. The charged (NH_3^+) and zwitterionic ABT forms, most probably dominant in many experiments, were sometimes not considered at all. In the present study, we compare the observed intensities to density functional computations, investigate the role of metal binding and protonation on the ABT absorption threshold, and model the effect of ABT dye orientation with respect to the metal surface. The simulations are primarily compared to experiments obtained on copper colloids and plates, where the monomeric ABT form prevails. On silver and gold, depending on experimental conditions, 4,4′-dimercaptoazobenzene ("dimer") may be formed by a photocatalytic coupling from two ABT molecules, which interferes with the ABT SERS signal.[11] In electrochemical surface-enhanced Raman scattering (EC SERS) spectroscopy, formation of the dimer can be avoided or limited by pH, potential, electrolyte composition, laser power, and surface feature variations.[12,13] De/protonation of ABT and activation of oxygen on the surface were also suggested as important factors in dimer formation.[11,14]

Traditionally, the SERS increase of Raman band intensities is attributed to the amplification of the laser electromagnetic field at the vicinity of metal nanostructured surfaces and particles ("plasmon resonance") and "chemical" changes of the absorbing species.[15] This can also be shown for ABT, where the computations given below suggest that the chemical bound to the metal increases absorption in the region of the laser excitation radiation and thus significantly contributes to the overall enhancement. Matrix polarization theory (MPT),[16,17] where the metal is modeled simply by a polarizable sphere, enables one to estimate the effect of molecular orientation on relative Raman intensities of individual vibrational bands.

METHODS

Experimental Raman and SERS Spectra. Experimental details related to sample preparation and measurement are described elsewhere.[4,12] Briefly, copper, silver, and golden surfaces were prepared by electrochemical metal coating of platinum targets. Cu nanoparticles were prepared using

Received: June 13, 2016
Revised: July 20, 2016
Published: July 25, 2016

DOI: 10.1021/acs.jpcc.6b05947
J. Phys. Chem. C 2016, 120, 18275−18280

aqueous sodium citrate solution reduced by copper sulfate in the presence of borohydride under an inert nitrogen atmosphere using a known procedure.[18−20] The ABT dye was then deposited on the surfaces from its saturated solution in methanol. Ordinary Raman spectra of ABT powder were measured with excitation wavelengths of 488, 785, and 1064 nm, and the Raman spectrum of 0.1 M methanolic ABT solution was measured with the 1064 nm excitation. If not said otherwise, targets' SERS spectra presented in this study were obtained in a spectroelectrochemical cell, in a 0.1 M aqueous K_2SO_4 solution (pH ≈ 7) and using the 785 nm excitation. The structure of the metal target surfaces is characterized in ref 4. No voltage was applied. Cu nanoparticles were kept in a quartz cell under a nitrogen atmosphere, and the 1064 nm laser was used. The spectra were acquired on the following instruments: disperse Raman spectrometer of LabRam, Dilor Jobin−Yvon, with a 488 nm argon ion laser and thermoelectrically cooled CCD, a Dimension P2 Raman spectrometer, Lambda Systems, with a 785 nm diode laser and thermoelectrically cooled CCD, and FT-Raman spectrometer Equinox 55/S, FRA106/S, Bruker, with a Nd:YAG 1064 nm excitation laser and a liquid-nitrogen-cooled germanium diode detector.

Density Functional Calculations. Geometries of neutral and zwitterionic ABT forms and the dimer (Figure 1) were optimized by energy minimization, and their spectra were calculated at the B3LYP/6311++G** level using the Gaussian 09, D01[21] program. ABT derivatives with one or several metal atoms were used to simulate the effect of binding to the metal. Such an approach has been used previously and successfully reproduced trends in chromophore spectroscopic properties upon binding.[22−24] For the Cu, Ag, and Au metals, the MDF10,[25] MWB28, and MWB60[26] pseudopotentials were used, respectively. Vacuum and the universal solvation model (SMD)[27] with methanol parameters were used for the environment. Time-dependent density functional theory (TD DFT)[28] was used to calculate excited electronic (singlet) states and absorption intensities. Raman spectra of crystalline ABT were alternatively simulated by the CASTEP program.[29] Here, periodic boundary conditions based on X-ray parameters,[30] ultrasoft pseudopotentials,[31] and a plane-wave cutoff energy of 300 eV were used. Note that ABT exists in the zwitterionic form in the crystal, as determined by X-ray, and has a high propensity to this form also in liquid.[30] At the surfaces, we used by default the protonated form of ABT (Cu-ABTH$^+$ etc.) because of the general stability of the charged form in crystal and neutral environments. In a real sample, one can suppose equilibrium of both forms; their Raman spectra, in any case, are quite similar in shape.[11]

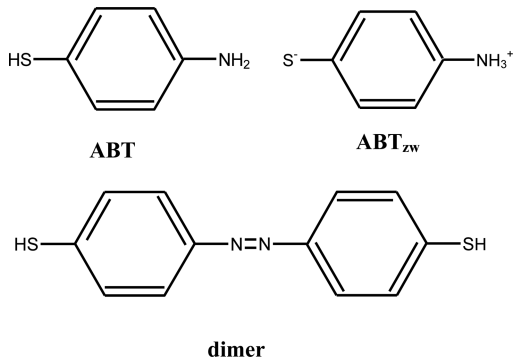

Figure 1. *p*-Aminobenzenethiol in nondissociated (ABT) and zwitterionic (ABT_{zw}) forms and the dimer.

Matrix Polarization Theory (MPT). Within MPT,[17] each particle of a system of chromophores (molecules and colloids) is represented by a polarizability, induced electric dipole, and higher moments.[16,32] Resultant time-dependent moments of the whole system are collected in a matrix **M** and can be obtained as $\mathbf{M} = \mathbf{P}\cdot(\mathbf{1} - \mathbf{X}\cdot\mathbf{P})^{-1}\cdot\mathbf{F}_0$, where the matrix **P** collects individual polarizabilities, **1** is a unit matrix, **X** is a tensor describing system geometry, and $\mathbf{F}_0$ is the intensity of the laser excitation.

In a simple case relevant for SERS, the matrix **M** contains dipole moments $\boldsymbol{\mu}_i$ and matrix **P** polarizabilities $\boldsymbol{\alpha}_i$. Particle i is either the dye or colloid; in the case of an experiment on the plate, the metal surface is just considered to be a large colloid. The dipole moments are induced by the electric field **E**, $\boldsymbol{\mu}_i = \boldsymbol{\alpha}_i\mathbf{E}_i$. The field at particle i consists of the laser field $\mathbf{E}_0$ and dipolar contributions from other particles, that is, $\mathbf{E}_i = \mathbf{E}_0 + \sum_{j\neq i}\mathbf{T}_{ij}\cdot\boldsymbol{\mu}_j$, where $\mathbf{T}_{ij} = (4\pi\varepsilon_0)^{-1}(3\mathbf{r}_{ij}\mathbf{r}_{ij} - \mathbf{1}r_{ij}^2)r_{ij}^{-5}$, $\mathbf{r}_{ij}$ is the difference of particle position vectors, and ε_0 is vacuum permittivity. As shown before,[33] it is the mutual particle polarization that can cause strong nonlinear SERS effects. The necessary condition is that the polarizability of one particle is large if (in atomic units) measured against r_{ij}^3.

MPT does not describe the chemical and resonance contributions to the enhancement explicitly but enables one to estimate the electromagnetic component of the dye−metal interaction and the dependence of SERS spectra on system geometry including molecular orientation, entering the total response to the electromagnetic radiation via the position tensor **T**. For this purpose, the metal surface or nanoparticle was approximated by a large polarizable sphere (polarizability = 4×10^6 au), placed in the vicinity of the ABT molecule. The molecule is represented by polarizability derivatives ("transition polarizabilities") calculated by Gaussian.

Backscattered Raman spectra were generated from the calculated intensities standard procedure,[32,34] using a temperature of 298 K for the Boltzmann correction factors and Lorentzian bands of 10 cm^{-1} full width at half maximum.

RESULTS AND DISCUSSION

Experimental Raman spectra of ABT powder and SERS observed on copper colloids and copper, silver, and gold nanostructured plates at 785 nm laser excitation are plotted in Figure 2. The ABT powder spectrum is similar to that obtained in methanol solution (Figure S1), indicating that the zwitterionic form of the compound is present also in the methanol polar solvent. This is consistent with the previous experimental and theoretical analyses showing that ABT prefers the zwitterionic form in crystal and liquid forms.[30] ABT spectra obtained at 488 and 1064 nm also plotted in Figure S1 do not significantly differ from the 785 nm curve in Figure 2. This suggests off-resonance Raman scattering for bare ABT because resonance of laser excitation light with electronic transitions of the free dye would lead to a signal boost and changes of relative band intensities.[35] For SERS spectra on colloids or metal plates, approximately 10^5-fold signal enhancement was achieved.

The interpretation of SERS observed on the copper surfaces is the most straightforward because here the dimer is not extensively formed. In Figure 2, one can observe that Cu colloids and plates provide very similar SERS spectra. Most Raman bands seen in the powder are apparent on the copper surfaces too, differing by minor intensity variations only (band

DOI: 10.1021/acs.jpcc.6b05947
J. Phys. Chem. C 2016, 120, 18275−18280

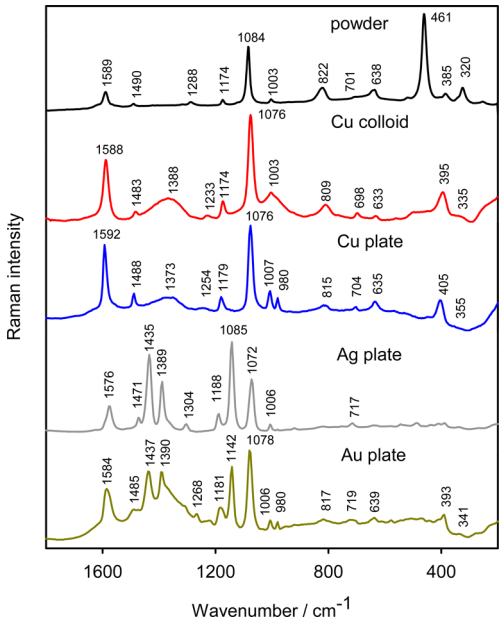

Figure 2. Experimental Raman spectra (785 nm excitation) of ATB powder and SERS at copper nanoparticles and copper, silver, and gold nanostructured plates (see ref 4 for experimental details). Raman intensities are normalized to the strongest peak.

positions in cm^{-1} for powder/plate SERS: 1589/1592, 1490/1488, 1174/1179, 1084/1076, 1003/1007, 822/815, 638/635). On the other hand, the strong 461 cm^{-1} band of the powder disappears in SERS, and a new band appears at 404 cm^{-1}.

The broad signal at around 1380 cm^{-1} on copper plates and colloids very much depends on experimental conditions. Most probably it stems from a presence of water under ambient conditions because it decreases under an inert atmosphere or system drying. Its properties can be studied using temperature- and humidity-controlled conditions, as shown in previous works.[36,37] For silver and gold plates, ABT dimer significantly contributes to SERS intensities in this region, as shown below.

First, however, to verify the computational methodology, we modeled the spectrum of pure (powder) ABT. Three approaches were adopted as presented in Figure 3. The ABT_{zw} zwitterionic form in vacuum (trace A in the figure) does not reproduce the experiment particularly well; for example, the relative intensity of the highest wavenumber signal at ~1590 cm^{-1} is underestimated, while the bands at 1464 and 652 cm^{-1} are too strong and so forth. The CASTEP computation (B) is technically the most appropriate one in that it includes the crystal periodicity and it also provides a much more realistic spectrum than the vacuum calculation. Similar intensity changes, however, can be achieved when the crystal environment of the zwitterion is simulated by the SMD continuous solvent model of methanol (C). Only the strongest band at 470 cm^{-1} in the experiment seems to be better reproduced by CASTEP but accidentally also by the vacuum calculation. Experimental and calculated frequencies of the strongest vibrational bands are summarized in Table 1. The assigned vibrations are consistent with previous computations for neutral ABT.[4,38]

The off-resonance Raman scattering on free ABT is not favorable for signal enhancement. However, dissociation to the zwitterion form and/or binding to the metal significantly increase the absorption threshold wavelength, as can be seen in

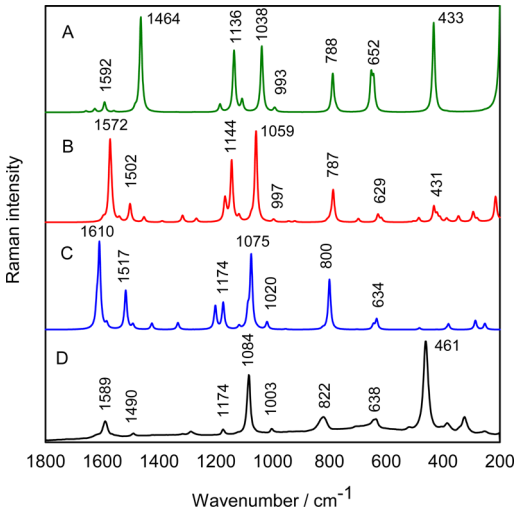

Figure 3. Raman spectra of the ATB_{zw} dye calculated for one molecule in vacuum (A), the CASTEP crystal calculation (B), calculation for one molecule within the methanol-like continuum solvent environment (C), and the experiment (D). The intensities are normalized to the highest peak.

Table 1. Calculated and Observed Frequencies and Assignment of the Strongest Raman and SERS Bands[a]

ABT Monomer				
ν_{cal}, ABT_{zw}	ν_{exp}, powder	ν_{cal}, Cu-$ABTH^+$	ν_{exp}, Cu plate	
1610−1636	1616	1624	1592	δ(N−H), scissor
1585	1589	1616	1592	δ(N−H), ν(C−C)
1517	1490	1517	1488	δ(N−H), umbrella
1333	1288	1335	1341	δ(C−H)
1174	1174	1179	1179	δ(C−H)
1075	1084	1085	1076	ν(C−S), δ(C−H)
1020	1003	1030	1007	δ(C−C−C)
800	822	807	815	δ(C−C), ν(C−N)
703	701	717	704	γ(C−H), γ(C−S)
634	638	623	635	ν(C−S), δ(C−C−C)
483	461	500	519	γ(C−H), γ(C−S)
381	385	382	405	δ(C−C−C)
286	320	342	335	γ(C−NH_3)
253	254	247	265	δ(C−S), δ(C−N)
ABT Dimer				
ν_{cal}, dimer	ν, Ag plate			
1622	1576	ν(C−C), ν(N−N)		
1505	1471	δ(C−C), δ(C−H), ν(N−N)		
1472	1435	ν(N−N), δ(C−H)		
1423	1389	ν(C−C), ν(N−N), δ(C−H)		
1339	1304	δ(N−C), δ(C−H)		
1229	1188	ν(N−C), δ(C−H)		
1161	1142	ν(N−C), δ(C−H)		
1085	1072	ν(C−S)		

[a] ν, stretching; δ, bending; γ, out of plane.

the absorption spectra plotted in Figure 4. The simulated absorption spectrum of ABT_{zw} is in a good agreement with the experiment in ref 39. At present, we are not able to simulate the metal bulk on an atomic level. Nevertheless, computations with a limited number of copper atoms suggest an important trend of increasing absorption in the laser excitation region,

DOI: 10.1021/acs.jpcc.6b05947
J. Phys. Chem. C 2016, 120, 18275−18280

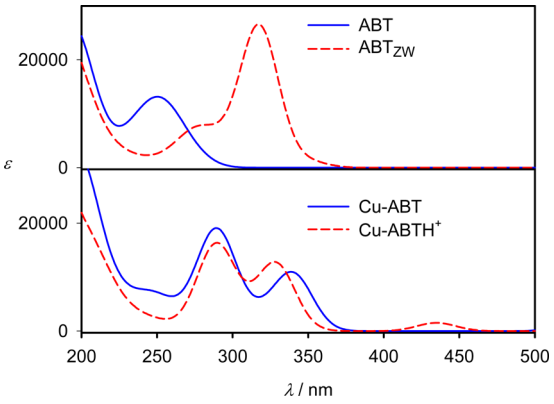

Figure 4. Calculated (B3LYP/6-311++G**/SMD(MeOH)) absorption spectra of ABT, ABT_{zw}, Cu-ABT, and Cu-ABTH$^+$.

explaining in part the enhancement of the Raman signal. Even though the laser excitation is not in direct resonance with electronic transitions of the dye, preresonance conditions can lead to a significant signal increase, too. The total enhancement is then a product of all of the contributing "chemical" and "electromagnetic" factors.[40,41]

A typical trend of the increase of the Raman intensities with the excitation energy is shown in Figure 5 for the signal at

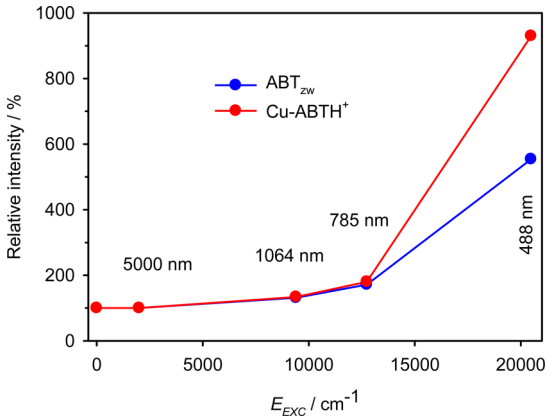

Figure 5. Calculated relative intensity (static case = 100%) of the 1610 cm^{-1} Raman band for five excitation wavelengths.

around 1610 cm^{-1} for the ABT_{zw} and Cu-ABTH$^+$ molecules. For Cu-ABTH$^+$ and the 488 nm excitation, the near-resonance increases the signal almost 10 times compared with the off-resonance scattering at $E_{EXC} \rightarrow 0$. The larger signal of Cu-ABTH$^+$ is consistent with the absorption spectra in Figure 4; in particular, the Cu-ABTH$^+$ absorption threshold (~440 nm) is closer to the 488 nm excitation than the ABT_{zw} one. Note that the electronic transitions seen in the absorption spectra enter computations of Raman intensities via frequency-dependent polarizability derivatives.[35]

The metal bulk itself as modeled by the polarizable sphere causes about a 10^3 increase of the Cu-ABTH$^+$ Raman signal (Figure 6). The neutral form (Cu-ABT, Figure S2) provides very similar spectra to Cu-ABTH$^+$. Although the sphere polarizability was estimated only approximately from a typical size of colloid particle or roughness of the plate surfaces,[4,42] together with occasional resonance or preresonance between the laser excitations, the bulk electromagnetic enhancement can well explain the observed effective enhancement values of ~10^5.

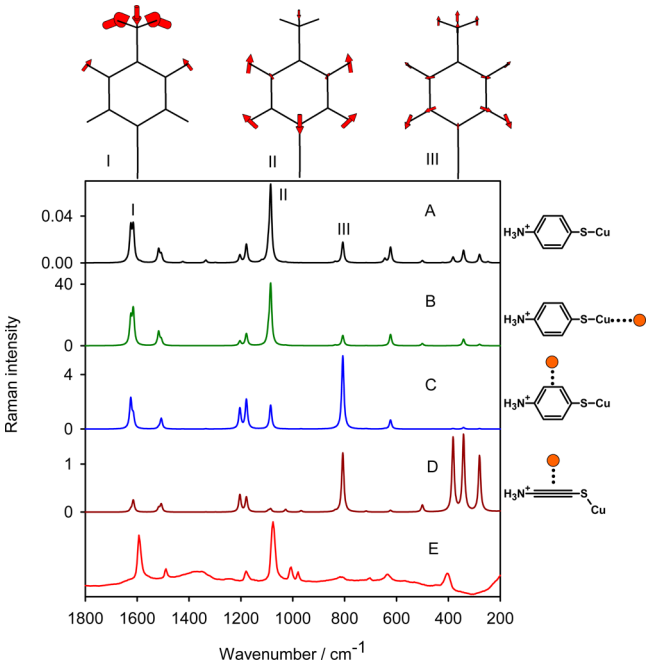

Figure 6. Raman Cu-ABTH$^+$ simulated for a single molecule (A) and in the presence of a polarizable sphere placed in the C–S bond direction (B), perpendicular to the C–S direction in the phenyl plane (C), and above it (D). For panels B–D, the MPT approach was used; (E) is the experiment on a Cu plate.

Comparing the computation to experiment, one should also consider that both the enhancement due to resonance of ABT electronic transitions with the laser excitation and the electromagnetic/plasma components are very dependent on the geometry and environment.[2,15,24,43] In a real sample, individual ABT molecules are supposed to experience different local environments and may exhibit significantly different enhancements.

When the metal is positioned along the molecular axis in the C–S bond direction (panel B, Figure 6), it does not significantly change relative intensities of Raman bands compared to bare ABT_{zw}. Polarizable spheres positioned perpendicular to the axis, in the benzene ring plane or above (panels C and D), change the relative intensities of Raman bands more. For example, in panel C, the intensity of the band at ~1085 cm^{-1} dramatically drops down. In this model, the "chemical" SERS effect is at least partially included via the attachment of the metal atom (cf. Figures 4 and 5). Clearly, the perpendicular positions are not very probable in experiment, both because of the disagreement of the simulated spectra with the observations and because of the obvious sterical constraints for ABT molecules bound to the metal via the sulfur atom. Unlike the hypothesis sometimes present in previous works,[8,44] we can see that although vibrations I–III have the same symmetry with respect to molecular axis they may be enhanced differently. For C and D, the presence of the sphere changes the symmetry of the whole system, which thus clearly seems more important than local symmetry with respect to a particular molecular residue.

Although a detailed analysis of the ABT dimer goes beyond the scope of the present study, its presence on the gold or silver surfaces can be confirmed by comparison of the simulated and experimental SERS as well. Theoretical spectra of the ABT monomer and dimer are plotted in Figure 7. Indeed, the

DOI: 10.1021/acs.jpcc.6b05947
J. Phys. Chem. C 2016, 120, 18275–18280

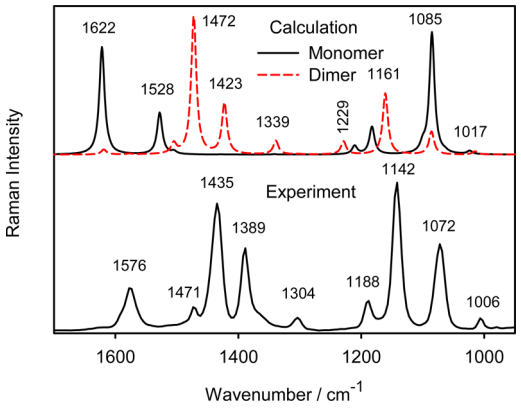

Figure 7. Simulated Raman spectra of Ag-ABTH$^+$ and the Ag-ABT−ABT-Ag dimer and the experiment on the Ag surface.

comparison of the simulation results with experimental intensities for silver and gold surfaces (Figure 2) suggests that both the molecular and dimerized ABT forms (in ∼1:2 ratio) are present in the real samples. As an additional computational check, we model ABT spectra for 1, 3, and 5 Cu atoms attached to it (Figure S3). Such variations in the number of metal atoms causes minor changes in the ABT vibrations (above 400 cm^{-1}) only; below 400 cm^{-1}, copper vibrational modes start to appear, which are in the experiment subtracted as a background. One can also notice that relative experimental intensities at lower wavenumbers are stronger than predicted, both for the monomer and dimer. This could not be explained by accuracy of the DFT computations or by the effect of molecular orientation and was attributed to an uneven enhancement across a wider spectral region in the experiment. Indeed, the silver plasmonic resonance quickly diminishes beyond the 785 nm excitation,[39] which makes the measured signal of high-wavenumber vibrations smaller.

CONCLUSIONS

We compared solid ABT Raman spectra and corresponding SERS spectra on copper, silver, and gold surfaces with density functional simulations combined with MPT in order to understand the experimental results obtained under various conditions. The modeling provided a good basis for understanding the experimental observations; the results suggest that observed enhancement of the Raman signal is a combination of enhancement stemming from resonance between the excitation radiation and ABT and metal electronic levels and electrodynamic enhancement due to the polarizable metal bulk. We also found that both protonated ABT forms (NH_3^+) and binding to the metal cause a red shift of the absorption threshold and favor the resonance of molecular energy levels with laser excitation. MPT also enabled us to model the dependence of relative Raman intensities on molecular orientation; the results suggest an almost perpendicular average orientation of the ABT dye to the metal surface, which is consistent with attachment to the surface through the sulfur atom.

ASSOCIATED CONTENT

Supporting Information

The Supporting Information is available free of charge on the ACS Publications website at DOI: 10.1021/acs.jpcc.6b05947.

Additional experimental and computational data, including Raman spectra of the species studied (PDF)

AUTHOR INFORMATION

Corresponding Author

*E-mail: bour@uochb.cas.cz. Telephone: (420) 220 183 348.

Notes

The authors declare no competing financial interest.

ACKNOWLEDGMENTS

The work was supported by the Grant Agency of the Czech Republic (Grant Numbers 13-03978S and 16-05935S).

REFERENCES

(1) Fleischmann, M.; Hendra, P. J.; McQuillan, A. J. Raman Spectra of Pyridine Adsorbed at a Silver Electrode. *Chem. Phys. Lett.* **1974**, *26*, 163−166.

(2) Schlücker, S. Surface-Enhanced Raman Spectroscopy: Concepts and Chemical Applications. *Angew. Chem., Int. Ed.* **2014**, *53*, 4756−4795.

(3) Čermáková, K.; Šesták, O.; Matějka, P.; Baumruk, V.; Vlčková, B. Surface-Enhanced Raman-Scattering (Sers) Spectroscopy with Borohydride-Reduced Silver Colloids - Controlling Adsorption of the Scattering Species by Surface-Potential of Silver Colloid. *Collect. Czech. Chem. Commun.* **1993**, *58*, 2682−2694.

(4) Dendisová, M.; Havránek, L.; Ončák, M.; Matějka, P. In Situ SERS Study of Azobenzene Derivative Formation from 4-Aminobenzenethiol on Gold, Silver, and Copper Nanostructured Surfaces: What Is the Role of Applied Potential and Used Metal? *J. Phys. Chem. C* **2013**, *117*, 21245−21253.

(5) Dendisová-Vyškovská, M.; Kokaislová, A.; Ončák, M.; Matějka, P. SERS and in Situ SERS Spectroscopy of Riboflavin Adsorbed on Silver, Gold and Copper Substrates. Elucidation of Variability of Surface Orientation Based on Both Experimental and Theoretical Approach. *J. Mol. Struct.* **2013**, *1038*, 19−28.

(6) Člupek, M.; Prokopec, V.; Matějka, P.; Volka, K. Raman Spectral Detection and Assessment of Thin Organic Layers on Metal Substrates: Systematic Approach from Substrate Preparation to Map Evaluation. *J. Raman Spectrosc.* **2008**, *39*, 515−524.

(7) Wu, D.; Liu, X.; Huang, Y.; Ren, B.; Xu, X.; Tian, Z. Surface Catalytic Coupling Reaction of p-Mercaptoaniline Linking to Silver Nanostructures Responsible for Abnormal SERS Enhancement: A DFT Study. *J. Phys. Chem. C* **2009**, *113*, 18212−18222.

(8) Osawa, M.; Matsuda, N.; Yoshii, K.; Uchida, I. Charge Transfer Resonance Raman Process in Surface-Enhanced Raman Scattering from p-Aminothiophenol Adsorbed on Silver: Herzberg-Teller Contribution. *J. Phys. Chem.* **1994**, *98*, 12702−12707.

(9) Wang, Y.; Chen, H.; Dong, S.; Wang, E. Surface-Enhanced Raman Scattering of Silver-Gold Bimetallic Nanostructures with Hollow Interiors. *J. Chem. Phys.* **2006**, *125*, 044710.

(10) Wu, D.; Zhao, L.; Liu, X.; Huang, R.; Huang, Y.; Ren, B.; Tian, Z. Photon-Driven Charge Transfer and Photocatalysis of p-Aminothiophenol in Metal Nanogaps: A DFT Study of SERS. *Chem. Commun.* **2011**, *47*, 2520−2522.

(11) Duan, S.; Ai, Y. J.; Hu, W.; Luo, Y. Roles of Plasmonic Excitation and Protonation on Photoreactions of p-Aminobenzenethiol on Ag Nanoparticles. *J. Phys. Chem. C* **2014**, *118*, 6893−6902.

(12) Dendisová-Vyškovská, M.; Prokopec, V.; Člupek, M.; Matějka, P. Comparison of SERS Effectiveness of Copper Substrates Prepared by Different Methods: What Are the Values of Enhancement Factors? *J. Raman Spectrosc.* **2012**, *43*, 181−186.

(13) Huang, Y. H.; Zhu, H. P.; Liu, G. K.; Wu, D. Y.; Ren, B.; Tian, Z. Q. When the Signal Is Not from the Original Molecule to Be Detected: Chemical Transformation of Para-Aminothiophenol on Ag During the SERS Measurement. *J. Am. Chem. Soc.* **2010**, *132*, 9244−9246.

(14) Huang, Y. F.; Zhang, M.; Zhao, L. B.; Feng, J. M.; Wu, D. Y.; Ren, B.; Tian, Z. Q. Activation of Oxygen on Gold and Silver Nanoparticles Assisted by Surface Plasmon Resonances. *Angew. Chem., Int. Ed.* **2014**, *53*, 2353−2357.
(15) Kleinman, S. L.; Ringe, E.; Valley, N.; Wustholz, K. L.; Phillips, E.; Scheidt, K. A.; Schatz, G. C.; Van Duyne, R. P. Single-Molecule Surface-Enhanced Raman Spectroscopy of Crystal Violet Isotopologues: Theory and Experiment. *J. Am. Chem. Soc.* **2011**, *133*, 4115−4122.
(16) Novák, V.; Šebestík, J.; Bouř, P. Theoretical Modeling of the Surface-Enhanced Raman Optical Activity. *J. Chem. Theory Comput.* **2012**, *8*, 1714−1720.
(17) Bouř, P. Matrix Formulation of the Surface-Enhanced Raman Optical Activity. *J. Chem. Phys.* **2007**, *126*, 136101.
(18) Sanchez-Cortés, S.; García-Ramos, J. V. Surface-Enhanced Raman Spectroscopy Study of 9-Ethylguanine and Related Compounds on Silver and Copper Colloids. *Vib. Spectrosc.* **1993**, *4*, 185−192.
(19) Sánchez-Cortés, S.; García-Ramos, J. V.; Morcillo, G. Morphological Study of Metal Colloids Employed as Substrate in the SERS Spectroscopy. *J. Colloid Interface Sci.* **1994**, *167*, 428−436.
(20) Ding, L. P.; Fang, Y. The Study of Resonance Raman Scattering Spectrum on the Surface of Cu Nanoparticles with Ultraviolet Excitation and Density Functional Theory. *Spectrochim. Acta, Part A* **2007**, *67*, 767−771.
(21) Frisch, M. J.; Trucks, G. W.; Schlegel, H. B.; Scuseria, G. E.; Robb, M. A.; Cheeseman, J. R.; Scalmani, G.; Barone, V.; Mennucci, B.; Petersson, G. A.; et al. *Gaussian 09*; Gaussian, Inc.: Wallingford, CT, 2009.
(22) Mohammed, A.; Hu, W.; Andersson, P.; Lundquist, M.; Landström, L.; Luo, Y.; Ågren, H. Cluster Approximations of Chemically Enhanced Molecule-Surface Raman Spectra: The Case of Trans-1,2-Bis (4-Pyridyl) Ethylene (BPE) on Gold. *Chem. Phys. Lett.* **2013**, *581*, 70−73.
(23) El-Khoury, P. Z.; Hess, W. P. Raman Scattering from 1,3-Propanedithiol at a Hot Spot: Theory Meets Experiment. *Chem. Phys. Lett.* **2013**, *581*, 57−63.
(24) Zhao, L.; Jensen, L.; Schatz, G. C. Pyridine-Ag_{20} Cluster: A Model System for Studying Surface-Enhanced Raman Scattering. *J. Am. Chem. Soc.* **2006**, *128*, 2911−2919.
(25) Figgen, D.; Rauhut, G.; Dolg, M.; Stoll, H. Energy-Consistent Pseudopotentials for Group 11 and 12 Atoms: Adjustment to Multi-Configuration Dirac−Hartree−Fock Data. *Chem. Phys.* **2005**, *311*, 227−244.
(26) Andrae, D.; Häußermann, U.; Dolg, M.; Stoll, H.; Preuß, H. Energy-Adjusted ab Initio Pseudopotentials for the Second and Third Row Transition Elements. *Theor. Chim. Act.* **1990**, *77*, 123−141.
(27) Marenich, A. V.; Cramer, C. J.; Truhlar, D. G. Universal Solvation Model Based on Solute Electron Density and on a Continuum Model of the Solvent Defined by the Bulk Dielectric Constant and Atomic Surface Tensions. *J. Phys. Chem. B* **2009**, *113*, 6378−6396.
(28) Furche, F.; Ahlrichs, R. Adiabatic Time-Dependent Density Functional Methods for Excited State Properties. *J. Chem. Phys.* **2002**, *117*, 7433−7447.
(29) Clark, S. J.; Segall, M. D.; Pickard, C. J.; Hasnip, P. J.; Probert, M. J.; Refson, K.; Payne, M. C. First Principles Methods Using CASTEP. *Z. Kristallogr. - Cryst. Mater.* **2005**, *220*, 567−570.
(30) Jetti, R. K. R.; Boese, R.; Thakur, T. S.; Vangala, V. R.; Desiraju, G. R. Proton Transfer and $N^{(+)}$−H···$S^{(-)}$ Hydrogen Bonds in the Crystal Structure of 4-Aminothiophenol. *Chem. Commun.* **2004**, 2526−2527.
(31) Vanderbilt, D. Soft Self-Consistent Pseudopotentials in a Generalized Eigenvalue Formalism. *Phys. Rev. B: Condens. Matter Mater. Phys.* **1990**, *41*, 7892−7895.
(32) Barron, L. D. *Molecular Light Scattering and Optical Activity*; Cambridge University Press: Cambridge, 2004.
(33) Janesko, B. G.; Scuseria, G. E. Surface Enhanced Raman Optical Activity of Molecules on Orientationally Averaged Substrates: Theory of Electromagnetic Effects. *J. Chem. Phys.* **2006**, *125*, 124704.
(34) Polavarapu, P. L. *Vibrational Spectra: Principles and Applications with Emphasis on Optical Activity*; Elsevier: Amsterdam, The Netherlands, 1998; Vol. *85*.
(35) Nafie, L. *Vibrational Optical Activity: Principles and Applications*; Wiley: Chichester, U.K., 2011.
(36) Kokaislová, A.; Helešicová, T.; Ončák, M.; Matějka, P. Spectroscopic Studies of Folic Acid Adsorbed on Various Metal Substrates: Does the Type of Substrate Play an Essential Role in Temperature Dependence of Spectral Features? *J. Raman Spectrosc.* **2014**, *45*, 750−757.
(37) Kokaislová, A.; Parchaňský, V.; Matějka, P. Surface-Enhanced Infrared Spectra of Nicotinic Acid and Pyridoxine on Copper Substrates: What Is the Effect of Temperature and Deposition Conditions? *J. Phys. Chem. C* **2015**, *119*, 26526−26539.
(38) Vidal-Iglesias, F. J.; Solla-Gullón, J.; Orts, J. M.; Rodes, A.; Pérez, J. M. Spectroelectrochemical Study of the Photoinduced Catalytic Formation of 4,4′-Dimercaptoazobenzene from 4-Aminobenzenethiol Adsorbed on Nanostructured Copper. *J. Phys. Chem. C* **2015**, *119*, 12312−12324.
(39) Santos, E. B.; Sigoli, F. A.; Mazali, I. O. Intercalated 4-Aminobenzenethiol between Au and Ag Nanoparticles: Effects of Concentration and Nanoparticles Neighborhood on Its SERS Response. *J. Braz. Chem. Soc.* **2015**, *26*, 970−977.
(40) Doering, W. E.; Nie, S. Single-Molecule and Single-Nanoparticle SERS: Examining the Roles of Surface Active Sites and Chemical Enhancement. *J. Phys. Chem. B* **2002**, *106*, 311−317.
(41) Valley, N.; Greeneltch, N.; Van Duyne, R. P.; Schatz, G. C. A Look at the Origin and Magnitude of the Chemical Contribution to the Enhancement Mechanism of Surface-Enhanced Raman Spectroscopy (SERS): Theory and Experiment. *J. Phys. Chem. Lett.* **2013**, *4*, 2599−2604.
(42) Prokopec, V.; Dendisová-Vyškovská, M.; Kokaislová, A.; Čejková, J.; Člupek, M.; Matějka, P. Spectroscopic Study of SERS- and SEIRA-Activity of Copper Large-Scaled Surface Substrates Prepared by Electrochemical Deposition: What Is the Role of Oxidation−Reduction Cycle Treatment? *J. Mol. Struct.* **2011**, *993*, 410−419.
(43) Šebek, J.; Kejík, Z.; Bouř, P. Geometry and Solvent Dependence of the Electronic Spectra of the Amide Group and Consequences for Peptide Circular Dichroism. *J. Phys. Chem. A* **2006**, *110*, 4702−4711.
(44) Moskovits, M.; Suh, J. S. Surface Selection Rules for Surface-Enhanced Raman Spectroscopy: Calculations and Application to the Surface-Enhanced Raman Spectrum of Phthalazine on Silver. *J. Phys. Chem.* **1984**, *88*, 5526−5530.

DOI: 10.1021/acs.jpcc.6b05947
J. Phys. Chem. C 2016, 120, 18275−18280